České Vysoké Učení Technické v Praze

Fakulta Stavební

Czech Technical University in Prague

Faculty of Civil Engineering

Ing. Michal Sněhota, Ph.D.

Non-invasive visualization methods for investigation of water flow and solute transport in porous media

Neinvazivní metody vizualizace proudění a transportu v pórovitém prostředí

Summary

Non-invasive imaging methods are being increasingly used in porous media research. Methods of magnetic resonance imaging, X-Ray computer tomography and neutron imaging are presented in the first part of the lecture. Potential of these methods for investigating the water flow and solute transport in porous media is discussed with focus on applications in soil physics. Examples of non-invasive imaging methods use for laboratory experimental studies on soil columns are given in the second part of the lecture. Noninvasive methods provided insight in processes causing flow instability in selected heterogeneous soils.

Souhrn

Neinvazivní vizualizační metody jsou stále více využívaným nástrojem při výzkumu procesů v pórovitém prostředí. Přednáška nejprve představuje principy metod rentgenové počítačové tomografie, neutronového snímkování a magnetické nukleární rezonance a dále se věnuje potenciálu uvedených metod ve výzkumu proudění vody a transportu rozpuštěných látek v porézním prostředí se zaměřením na aplikace v půdní fyzice. V druhé části přednášky jsou uvedeny příklady využití neinvazivních snímkovacích metod pro laboratorní experimentální výzkum proudění na půdních válcových vzorcích. Při těchto experimentech neinvazivní metody přispěly k lepšímu pochopení nestability proudění pozorované v některých heterogenních půdách.

Klíčová slova:

nukleární magnetická resonance, počítačová tomografie, neutronová radiografie, preferenční proudění, půda

Key words:

nuclear magnetic resonance, computed tomography, neutron radiography, preferential flow, soil

Table of contents

1. Introduction 6

2. Non-invasive visualization techniques theory 7

3. Aplications of visualization techniques for studies of flow and transport in porous media 13

4. Summary and outlook..... 20

5. Acknowlegements 20

6. References 21

1. Introduction

Subsurface hydrological processes are not accessible for direct visual observation. The flow and transport bellow surface is generally inspected on basis of point measurements or on subsamples, which often represent only a tiny fraction of a flow domain. At the same time, soils as results of complex soil formation processes are often heterogeneous at a wide range of scales with direct impact on the water flow distribution.

When standard quantities i.e. water content, pressure head, solute concentration or temperatures are sampled only in limited number of discreet points, the monitoring may not provide a relevant picture of the flow or transport processes. For example, studying the phenomenon of the preferential flow, in which the majority of water flow is conducted only through a small portion of the flow domain (fracture) at substantially higher velocities than in the rest of the soil (matrix), the interpretation of pressure head measured by a tensiometer can be blurred. Depending on the size and position of the tensiometer ceramic cup, the values may represent the pressure in the matrix domain itself or some combination of pressures in the fracture and matrix domains (Finsterle and Faybishenko, 1998). Similar concerns apply also to the water content measurements. Furthermore, the installation and operation of probes in the soil profile present a physical impact on the soil integrity and may influence the nature of flow processes. For example, pressure and flow fields in the vicinity of a suction cup are changed during the water extraction for chemical analysis.

To overcome these limitations non-invasive imaging methods has been increasingly used in the porous media research. Non-invasive methods allow direct observation or imaging of the porous media and the flow and transport processes occurring within them.

This lecture presents non-invasive methods recently used to study the porous media with a special focus on methods that has been successfully used for monitoring flow and transport processes in a natural porous medium – the soil.

2. Theory of selected non-invasive visualization techniques

2.1 X-ray tomography

The computer axial tomography (CAT) or computer tomography (CT) is based on measuring the attenuation of the x-ray (or gamma) beam in a sample. The method was developed as a medical diagnostic technique (Hounsfield, 1973). Due to its excellent ability to reveal the spatial distribution of the inner structure of objects, the method soon became frequently used in industrial and research applications.

The X-ray computer tomography imaging maps the distribution of linear attenuation coefficient over an entire transverse section of a sample. Once an X-ray beam of energy of 30 - 200 keV, which is the energy range of present-day tomographs, penetrates the sample, the beam is attenuated by its interactions with matter in processes of coherent scattering, photoelectric scattering and Compton (incoherent) scattering. The linear attenuation coefficient μ [L^{-1}] then depends on the effective atomic number Z_{ef} and the density ρ of the sample. The attenuation of a well-collimated X-ray beam follows the Beer's law:

$$I = I_0 e^{-\mu d} \qquad [1]$$

where I_0 is the intensity of the incident X-ray photons, I is the intensity transmitted through the sample, d [L] is the sample width. Equation [1] is valid for a homogeneous sample. The sample of porous media consists of solid, liquid and gas phases of various different attenuation coefficients. Then the beam intensity behind the composite sample is:

$$I = I_0 e^{-\int \mu(x) dx} \qquad [2]$$

When energy of the X-ray beam is higher than 100 keV, the Compton effect prevails, and the linear attenuation coefficient μ depends predominantly on the sample density and not on its chemical composition.

The product μx is determined by measuring the attenuation of a thin beam of radiation, with a constant distance between the beam source and the detector. The attenuation is measured in a finite number of coplanar directions. The two dimensional image (slice) is then reconstructed by appropriate reconstruction algorithm. The image slice of a thickness equal to the beam width, represents the matrix of linear attenuation coefficients expressed as image intensities. The three-dimensional (3D) image then consists of series of slices.

The image intensities are usually given in Hounsfield units (HU), which is the convenient linear transformation of μ in most cases calibrated to obtain 0 HU for the density of air and +1000 HU for density of water. The local macroscopic porosities can be calculated from HU for images obtained by scanning of completely dry sample (see e.g. Císlerová and Votrubová, 2002).

During past two decades computer tomography has been increasingly used in research fields of subsurface hydrology, soil physics and related sciences. The applications involved measurements of spatial and temporal variability of soil water content and porosity (Hopmans et al., 1994), estimation of flow domains in soils with preferential flow (Císlerová and Votrubová, 2002), visualization and characterization of macropores in intact soil samples (e.g. Perret et al., 1999), the influence of the vegetation cover (Rachman et al., 2005) on soil structure. X-ray computer tomography can be also effectively used to assess disturbance of intact soil cores for column experiment (Pires et al., 2004; Sněhota et al., 2005; Sněhota et al., 2010).

2.2 Neutron imaging

Neutron imaging (NI) theory is very similar to the theory of imaging using the X-rays. In NI however the sample is penetrated by neutron beam. When neutron beam passes through a sample, neutrons interact with atomic nucleus in manner which varies greatly with isotopic composition and neutron energy. Energy levels of thermal and cold neutrons are used most frequently for imaging.

In contrast to the X-rays, which interact with electrons and heavy materials induce strong attenuation, no dependence of attenuation coefficient on atomic number exists for thermal and cold neutrons. Many light elements including hydrogen causes strong neutron scattering while other heavier materials are relatively transparent for neutrons. This makes neutron imaging very particularly suitable for studies of water flow in porous media.

Neutron imaging techniques available for porous media investigation are the neutron radiography (NR), which is suitable for real-time monitoring of processes in a sample, and neutron tomography (NT) for imaging with output image resolved in three dimensions.

For neutron radiography a sample is placed in the parallel, highly collimated neutron beam in front of the two dimensional detector. The neutron beam passes through the sample and it is captured in a detector. The result is an image of gray levels representing the beam intensity.

For simple case of soil sample enclosed in glass container, the beam intensity of the transmitted neutron through the sample is described by the attenuation law (Carminati, et al., 2007)

$$-\ln\left(\frac{I(x,z,t)}{I_0(x,z)}\right)=\Sigma_w L_w(x,z,t)+\Sigma_{soil}L_{soil}(x,z)+\Sigma_{cyl}L_{cyl}(x,z) \qquad [3]$$

where (x,y) is the plane perpendicular to the neutron beam direction , t is the time, I_0 and I are the in-coming and out-going neutron beam intensities, L is the thickness in the beam direction, and Σ are the linear attenuation coefficients of the materials contained in the sample (suffix “cyl” is for cylinder, “soil” is for soil material and “w“ is for water. The negative logarithm in the equation [3] represents the image intensities normalized to the open beam image (without the presence of a sample) and products $\Sigma_{soil}L_{soil}(x,z)+\Sigma_{cyl}L_{cyl}(x,z)$ can be obtained from the image of a dry soil. With the known attenuation coefficient of water Σ_W [L^{-1}] and the known thickness of the sample d [L], the water content map can be calculated as:

$$\theta(x,z,t) = \frac{L_w(x,z,t)}{d} \qquad [4]$$

In some cases a correction for scattered neutrons must be employed (Hassanein et al., 2005).

Similarly to the X-ray computed tomography the neutron tomography is based on acquisition of series of radiographs taken while sample is rotated by 180° or 360° around its vertical axis. The three-dimensional image then can be obtained by inverse Radon algorithm (Vontobel et al., 2006).

The number of neutron sources and imaging beamlines in the world is still limited. An example of the beamline operated at the spallation neutron source SINQ (Paul Scherrer Institute, Switzerland) is shown in Fig. 1. For a detailed description of the neutron imaging theory and an overview of available neutron sources see Lehmann, (2009).

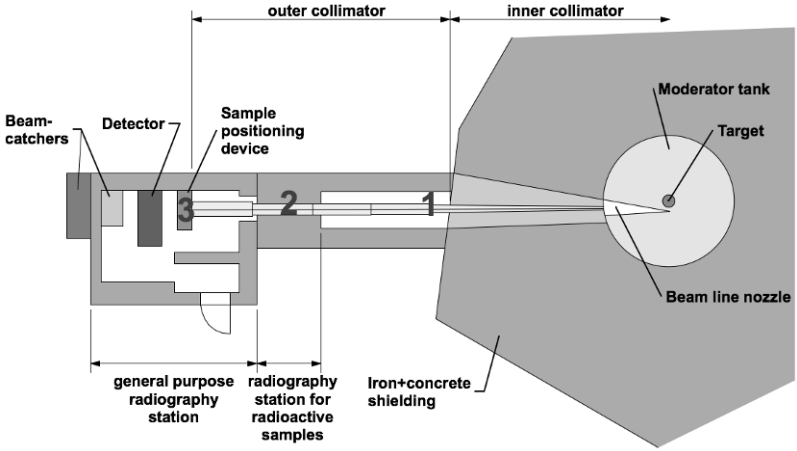

Figure 1: Schematic of NEUTRA beamline at spallation neutron source SINQ in Paul Scherrer Institute (Source: Paul Scherrer Institute)

2.3 Magnetic resonance imaging

For an MRI experiment, a sample is placed in a large, static homogeneous magnetic field where it is exposed to a series of radio frequency (RF) pulses; the subsequent emission of RF radiation from the resonating hydrogen proton nuclei (spins) within the sample is detected as the MR signal characterized by its amplitude, frequency, phase and duration of resonance (relaxation time). Sequences of various RF pulses have to be applied to measure specific MR parameters including the relaxation times *T1* (longitudinal, spin-lattice, recovery time) and *T2* (transversal, spin-spin, decay time) and proton density (spin density) M_0. The "spin-echo" pulse sequence is often used MRI of soil.

For given TR and TE of the pulse, the echo signal intensity is then:

$$I(TR,TE) = M_0\left(1 - e^{-TR/T1}\right)\left(e^{-TE/T2}\right) \qquad [5]$$

Although the MR signal detected by MRI comes from the hydrogen protons of each water molecule within the soil sample, not all of them produce an equal signal. The signal intensity (or M_0) of water in large pores is expected to be the highest. Both, the longitudinal relaxation time (*T1*) and the transversal relaxation time (*T2*) are dominated by relaxation at facial surfaces and are sensitive to pore size (Kleinberg et al., 1994). Consequently in larger pores filled by reasonable amounts of water protons the decay of the water-proton signal will be close to the decay of bulk water. Using encoding, the signal is resolved spatially and the result is the 2D or 3D image matrix (see Fig. 2). Fundamentals of MRI can be found elsewhere (e.g. Hashemi and Bradley, 2004).

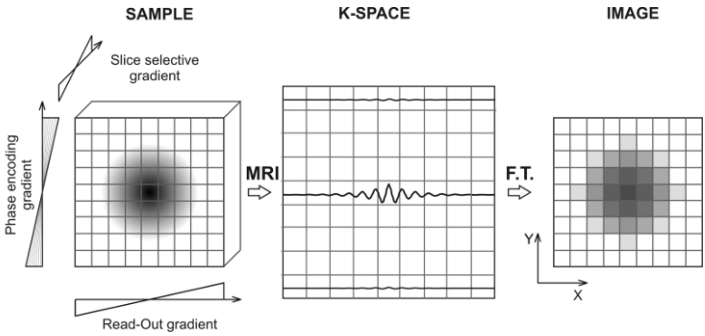

Figure 2: Schema of gradient encoding and 2D image reconstruction in MRI. The slice selective magnetic field gradient allows spins to resonation only in a slice of given depth and thickness. Series of bulk MR signals is acquired while two additional magnetic field gradients are incorporated in the pulse sequence. The series of signals (echoes) fills the K-Space. The image is then reconstructed by Fourier transform of the K-Space.

A large amount of work has been done in NMR/MRI of sedimentary rocks, a review is given by Kleinberg et al, (1994) or later by Song et al., (2008); unfortunately not all of these findings are relevant to MRI of soils. Amin et al., (1997), Hall et al., (1997) and Votrubová et al., (2000) presented crucial constraints for a wide range of soils and gave a comprehensive literature review. Based on the fact that for some natural soils only water in large pores produces a significant MR signal, MRI studies of preferential flow in undisturbed samples of heterogeneous soil were performed (Císlerová at al, 1999; Votrubová et al, 2003; Sněhota et al., 2010). Recently MRI was used to investigate the fate and transport of NAPLs (e.g. Chu, et al., 2004), to study the finger flow in sand (Posadas et al., 2009), to trace the transport of D_2O (Pohlmeier et al., 2009) and the transport of $Ni(NO_3)_2$ (Jelínková et al., 2011 in print).

3. Applications of visualization techniques for studies of flow and transport in porous media

3.1 X-ray computer tomography

The hydraulic characterization of soils, which is needed to simulate mathematically the water flow and solute transport, is traditionally conducted on intact columns of various sizes. The coefficient of the saturated hydraulic conductivity can be measured in infiltration-outflow experiments. Coupling the infiltration experiment data with the inverse numerical modeling, the estimation of parameters of soil characteristic curve (retention curve) is also feasible. The solute transport properties such as the dispersivity and sorption can be also tested on columns in column tracer breakthrough (BTC) tests. The success of soil characterization depends greatly on the understanding the inner structure of a soil sample and on the representativeness of given soil column, namely on its intactness. The presence of cracks caused by the sample extraction in the field may cause the flow bypassing and to bias the results significantly.

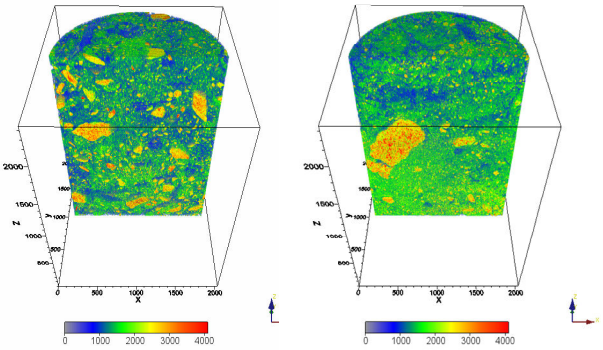

Figure 1: CT images of samples LIZ (left) and UHL (right). The color bar shows the HU values HU. The yellow and red colors represent stones, the green color show the soil matrix and blue color highlightes the least dense parts of the samples.

The soil physics laboratory at the Czech Technical University in Prague, Faculty of Civil Engineering, operates the semi-automated setup for conducting the infiltration-outflow and BTC experiments on large soil columns.

In study of temporal variability of hydraulic properties, soil samples from Liz (Šumava mountains, sample "LIZ") and Uhlířská (Jizera mountains, sample "UHL") watersheds were tested. Soil samples were scanned at standards CT medical scanner Siemens Somatom Plus IV. The output is three-dimensional (3D) image 512 x 512 x 246 and resolution of 400 x 400 x 1000 μm. Fig. 3 depicts the images visualized in 3D.

Detailed inspection of the images revealed that structure of the inner parts of soil samples was nearly intact, but gaps near to the sample walls were detected. Subsequently, a technique to seal the sample along the walls was developed and it is henceforth routinely used in our experiments.

The sample for the infiltration-outflow experiment is equipped with tensiometers for pressure head monitoring and TDR probes for sensing the water content. The probes must be physically inserted into the soil. Advantage of having CT image of studied sample available is then twofold: (1) installing the probes in carefully pre-selected position on the basis of CT image reduces the probability of probe collision with gravel grains comparing to the previously used "trial and error" method (2) knowledge of the soil geometry of particular probe's neighborhood and its orientation to preferential pathways in the sample helps to later interpret the probe measurements. Example of images that were used for planning for the tensiometer installation is shown in Fig. 4. Potential preferential pathways were identified by segmentation of the least dense parts of the sample.

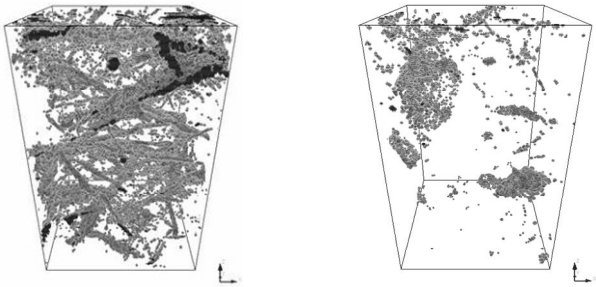

Figure 2: Potential preferential flow pathways of the samples LIZ (left) and UHL (right), identified by the image segmentation by tresholding and morphological pore opening.

3.2 Magnetic resonance imaging

The magnetic resonance imaging is capable to monitor free water in large soil pores, therefore it represent a highly applicable technique for studies of the preferential flow in soils. Fig. 5 illustrates the interpretation of the MRI measurements in example in which the MRI intensity image is compared with the results of other visualization techniques applied to the same soil sample.

The results of dye tracing (Brilliant Blue dye), CT and MRI are compared for the horizontal plane at the height of 6 cm above the sample bottom. Stained areas, which are marked with transparent blue color, show the regions of preferentially flowing water. As expected, it can be seen that water flowed generally in the regions of lower CT densities i.e. higher porosities especially through the loose structures and along large pores and cavities. In the MRI image, the highest signal intensities represent the largest amounts of MR-visible water. Due to inevitable distortions of MRI image it is impossible to perform direct pixel-to-pixel comparison of MRI and CT images (Votrubová et al., 2003) however the visual comparison gives the basic idea about the MRI information. There is reasonable

agreement between the occurrence of regions of high MR signal and regions of high porosity in CT images. It is also apparent that the non-stained regions produced very little MR signal. It is therefore reasonable to assume that MR-visible water is water present in large pores and holes.

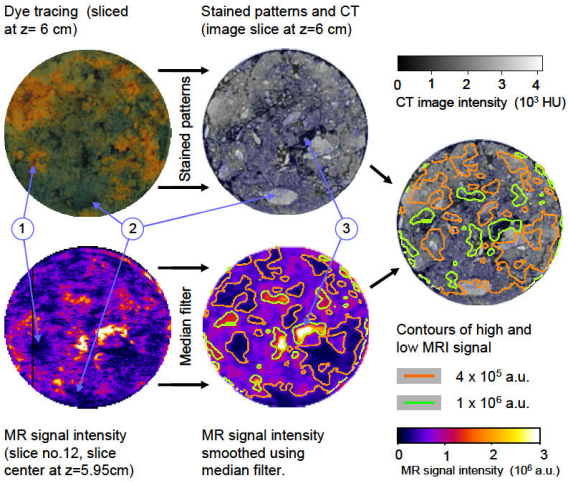

Figure 5: Comparison of the MR intensity image, CT image and the dye-tracing photograph. Complete overlay of the low and high MR signals map, CT image and stained patterns are shown on the right. Three different effects are numbered as follows: (1) non-stained region corresponds to the region without MR-visible water (2) stone imprint in the photograph of dye pattern is well visible in the CT image slice and is also reproduced as low-signal region in MR image, (3) larger cavity becomes filled with (free) water and produces high MR signal. (Sněhota et al, 2010)

The above interpretation of the MRI outputs was used in study of the water flow in heterogeneous coarse sandy loam soil from Korkusova Huť (Šumava). The soil under study exhibits significant temporal variations of the saturated hydraulic conductivity (see Císlerová et al, 1990), which can not be mathematically simulated using the standard theory. MRI was employed to study the process of infiltration in an undisturbed core of KH soil during the course of repeated ponded experiment (RPI), in which the

first infiltration was conducted in a naturally dry sample and the second infiltration was done into wet sample only drained by gravity. The results of MRI measurements helped to formulate the hypothesis about the entrapped air formation and redistribution during the course of RPI with direct impact on the hydraulic conductivity of the sample (Sněhota et al., 2010).

MRI was also used for real-time monitoring of the transient flow in soil sample (see Fig. 6). In the image annotated as $I_1p(t_0)$), which was taken before the infiltration beginning, the soil sample did not contain virtually any MR-visible water, even when the water content was relatively high (0.36 cm^3cm^{-3}).

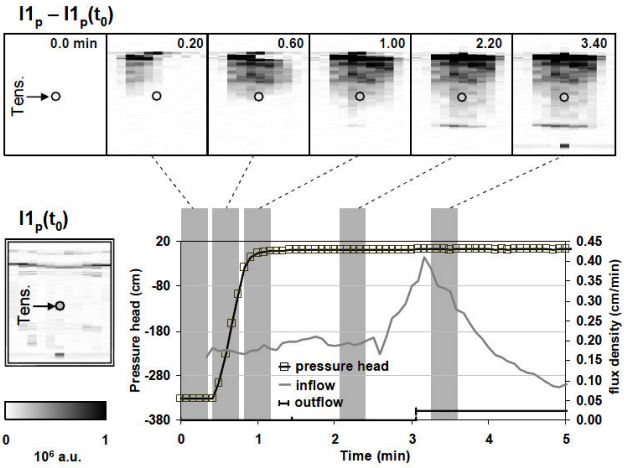

Figure 6: Comparison of measured flux rates and pressure heads with MRI images during initial 5 minutes of the infiltration. The acquisition period for each image is shown as a shaded bar. The image labeled $I1_p(t_0)$ show MR signal intensities (a.u.) before the first and second infiltration, respectively. Series of images $I_1p(t)$ show changes of signal intensities in time, where the image of "dry" sample $I_1p(t_0)$ was subtracted (Sněhota et al, 2010)

The advancement of the wetting front during the infiltration, visualized by MRI corresponds very well with the tensiometer records (tensiometer position is marked with circle). MR images show that water initially flooded the left part of the sample, then in time of ~ 0.2 min the wetting front reached the central part of the sample. As visible from images, the rate of the water supply at the top was not sufficient at the beginning. The sample surface flooded at time 1 - 2 min after the beginning of infiltration. At time 1.0 minute first water arrived to the perforated plate at the bottom of the sample.

3.3 Neutron imaging

In the third example the neutron imaging was utilized to support the hypothesis of air trapping and entrapped air redistribution in heterogeneous soil with subsequent reduction of the steady state flow rate during long-running infiltration into initially dry soil sample. Direct identification and visualization of entrapped bubbles in the KH soil was achieved in this experiment. The experiment was conducted at the NEUTRA beamline, connected to the SINQ neutron spallation source at Paul Scherrer Institute.

Undisturbed samples were carefully collected in KH site at the depth of 40 cm in the B horizon into quartz glass tubes (inner diameter 34 mm, length 100 mm). Total number of ten samples was collected. All samples were imaged by the X-ray tomography to reveal their inner structure. The two most representative and least disturbed samples were selected for the infiltration-outflow experiments with concurrent neutron imaging.

Series of neutron tomography images has been acquired during the steady state flow stage of the infiltration-outflow experiment. The image acquisition setup included the LiFe 100 μm scintillator plate coupled with cooled CCD camera. Each 3D image was reconstructed from 201 projections, where acquisition time for each projection was 7 seconds, making the total acquisition time needed to obtain a 3D image close to 30 minutes. The resulting dataset consists of series of 3D isotropic images with voxel size of 110 μm.

Infiltration outflow experiments were conducted in fully automated set-up with controlled level of ponding at the top of the sample and infiltration and outflow rates monitoring. For the first sample the hydraulic conductivity during the steady state flow stage of the experiment exhibited significant decline (from 3.0×10^{-5} m.s^{-1} to only 9.1×10^{-6} m.s^{-1}), which contradicts the standard theory. This behavior was however expected for soil under study. The hydraulic conductivity remained substantially lower, but relatively steady throughout the infiltration conducted on the second sample.

Neutron tomography images were analyzed in order to identify the air phase in the first sample. Under given boundary condition of current experiment the air phase present in the sample during the steady state stage of the experiment must be considered to be discontinuous from the atmosphere i.e. it represent the entrapped air. Reconstructed 3D images were firstly treated with a median filter to reduce noise and secondly were segmented by thresholding to extract voxels representing the entrapped air.

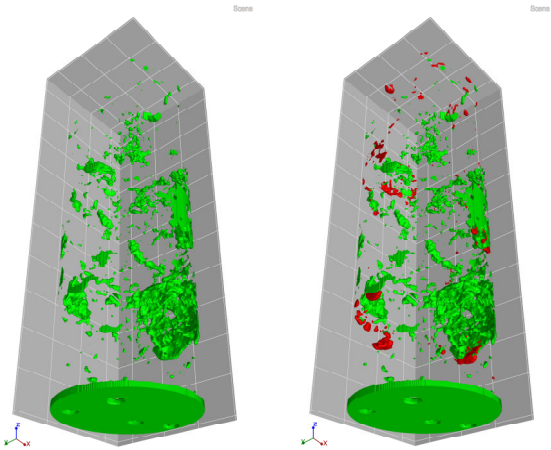

Figure 3: Visualization of entrapped air blobs in neutron tomography images aproximately 1 hour after beginning of infiltration experiment (picture on the left). Newly developed air bubbles (picture on the right) are shown in red color in the image acquired after 12 hours of infiltration.

The segmentation results are shown in Figure 7, where blobs of the entrapped air are visible in images taken 1 hour and 12 hours after the beginning of infiltration.

Quantifying the volume of NT detectable bubbles, we found that the increase of the entrapped air volume fraction from 1.6% to 2.3% reduced the hydraulic conductivity of the soil sample by more than 50%.

4. Summary and outlook

The noninvasive visualization methods MRI, X-ray CT and NT presented in the first part of this lecture helped to elucidate the effect of the entrapped air redistribution on quasi-saturated flow processes. Series of NT images taken during the quasi-steady state flow during the infiltration confirmed that the air trapping occur in many of large pores and cavities. Further air redistribution has been detected during later stages of the experiment. Experimental results supported the hypothesis that the effect of the gradual decrease of the flow rates is caused by the entrapped air redistribution and by the gradual build-up of bubbles in preferential flow pathways. The trapped air may thus restrict the preferential flow and cause the overall lower infiltration and outflow rates. The experiment results achieved with assistance of noninvasive visualization methods contribute to the ongoing research on flow instabilities in porous media.

5. Acknowledgements

The research of flow instabilities has been supported by GAČR under project no. 103/08/1552. The neutron imaging in PSI has been supported by PSI under project numbers 20100526, 20090465 and by „European Commission under the 7th Framework, Programme through the 'Research Infrastructures' action of the 'Capacities' Programme, contract No: CP-CSA_INFRA-2008-1.1.1 Number 226507-NMI3". MRI measurements were conducted in HSLMC, University of Cambridge, UK and ICGIII, Forschungzentrum Jülich, SRN. The habilitation thesis preparation was supported by MŠMT, project RP.

6. References

AMIN, M.H.G., HALL, L.D., CHORLEY, R.J., RICHARDS, K.S., CARPENTER, T.A., CÍSLEROVÁ, M. AND VOGEL, T., Study of infiltration into a heterogeneous soil using magnetic resonance imaging. Hydrol. Processes 11: 471-483, 1997.

CARMINATI, A, KAESTNER, A., HASSANEIN, R. IPPISCH, O., VONTOBEL, P., FLÜHLER H.: Infiltration through series of soil aggregates: Neutron radiography and modeling, Advances in Water Resources 30, 1168–1178, 2007.

CHU, Y.J., WERTH, C.J., VALOCCHI, A.J., YOON, H. AND WEBB, A.G., Magnetic resonance imaging of nonaqueous phase liquid during soil vapor extraction in heterogeneous porous media. Journal of Contaminant Hydrology 73(1-4): 15-37, 2004.

CÍSLEROVÁ, M., VOGEL, T. AND ŠIMŮNEK, J., The infiltration-outflow experiment used to detect flow deviations. In: Roth, K., Flühler, H., Jury W.A. and Parker, J.C. (eds.) Field-scale water and solute flux in soils. Bikhauser Verlag, Basel, 109-117. 1990.

CÍSLEROVÁ M., VOTRUBOVÁ J. CT derived porosity distribution and flow domains. Journal of Hydrology 267:186-200, 2002

FINSTERLE S., FAYBISHENKO B.: What does the tensiometer measure in fractured rock?, In: Characterization and measurement of the hydraulic properties of unsaturated porous media, Riverside, CA, 1998

HASSANEIN, R., LEHMANN, E., VONTOBEL, E., Methods of scattering corrections for quantitative neutron radiography. Nuclear Instruments and Methods in Physics Research A, 542, 353–360, 2005

HALL, L.D., AMIN, M.H.G., DOUGHERTY, E., ŠANDA, M., VOTRUBOVÁ, J., RICHARDS, K.S., CHORLEY, R.J. AND CÍSLEROVÁ, M., MR properties of water in saturated soils and resulting loss of MRI signal in water content detection at 2 tesla. Geoderma 80(3-4): 431-448., 1997.

HASHEMI, R.H. AND BRADLEY, W.G., MRI the basics. Lippincott Williams and Wilkins. 2004,

HOPMANS, J.W., CÍSLEROVÁ, M., AND VOGEL, T., X-Ray Tomography of Soil Properties. In: Tomography of Soil-Water-Root Processes, SSSA Special publication no. 36. SSSA, Madison. 1994.

HOUNSFIELD, G.N., A method and an apparatus for examination of a body by radiation such as x-or gamma radiation. British patent no. 1,283,915, London, 1972.

JELINKOVÁ V., SNĚHOTA, M., POHLMEIER A., VAN DUSSCHOTEN D., CÍSLEROVÁ M., Effects of entrapped residual air bubbles on tracer transport in

heterogeneous soil: Magnetic resonance imaging study. Organic Geochemistry, 2011 (in print).

KLEINBERG, R.L., KENYON, W.E., MITRA, P.P., mechanism of NMR relaxation of fluids in rock. Journal of Magnetic Resonance Series A 108(2): 206-214 1994.

LEHMANN, E.H. Neutron imaging methods and applications, In: Liang et al. (ed.), Neutron Applications in Earth, Energy and Environmental Sciences, Springer Science+Business Media. pp. 319 – 348, 2009

PERRET, J., PRASHER, S.O., KANTZAS, A., AND LANGFORD, C. Three-dimensional quantification of macropore networks in undisturbed soil cores . Soil Sci. Soc. of Am. J. 63: 1530-1543. 1999.

PIRES L.F., BACCHI O.O.S., REICHARDT K. Damage to soil physical properties caused by soil sampler devices as assessed by gamma ray computed tomography. Australian Journal of Soil Research 42:857-863. 2004.

POSADAS, A., QUIROZ, R., TANNUS, A., CRESTANA, S. AND VAZ, C.M., Characterizing water fingering phenomena in soils using magnetic resonance imaging and multifractal theory. Nonlinear Processes in Geophysics 16(1): 159-168, 2009.

POHLMEIER, A., VAN DUSSCHOTEN, D., WEIHERMÜLLER, L., SCHURR, U., VEREECKEN, H., Imaging Water Fluxes in Porous Media by Magnetic Resonance Imaging using D2O as a tracer. Magnetic Resonance Imaging 27(2): 285-292, 2009.

RACHMAN A., ANDERSON S.H., GANTZER C.J. Computed-tomographic measurement of soil macroporosity parameters as affected by stiff-stemmed grass hedges. Soil Science Society of America Journal 69:1609-1616, 2005.

SNĚHOTA M., DOHNAL M., CÍSLEROVÁ M., TESAŘ M. (2005) Velké neporušené vzorky ze dvou horských povodí: Infiltrační experimenty a snímky počítačovou tomografií, Hydrologie malého povodí 2005, Ústav pro hydrodynamiku AVČR, Praha. pp. 271 – 278

SNĚHOTA M., CÍSLEROVÁ M., AMIN M.H.G., HALL L.D. (2010) Tracing the Entrapped Air in Heterogeneous Soil by Means of Magnetic Resonance Imaging. Vadose Zone Journal 9:373-384. (2010)

SONG, Y.-Q., H. CHO, T. HOPPER, A. POMERANTZ, AND P. Z. SUN, Magnetic resonance in porous media: Recent progress. J. Chem. Phys. 128: 052212, 2008.

VONTOBEL P., LEHMANN, E.H., HASSANEIN, R., FREI G. Neutron Tomography: Method and Applications. Physica B-Condensed Matter 385:475-480, 2006

VOTRUBOVÁ, J., CÍSLEROVÁ, M., AMIN, M.H.G. AND HALL, L.D., Recurrent ponded infiltration into structured soil: a magnetic resonance imaging study. Water Resources Research 39(12): 1371, 2003.

Ing. Michal Sněhota Ph.D.

Date of birth: 22. 4. 1975

Email: michal.snehota@fsv.cvut.cz

Education

2000 Ing., Faculty of Civil Engineering, Czech Tech. Univ., Prague, Czech Republic

2003 Ph.D., Faculty of Civil Engineering, Czech Tech. Univ., Prague, Czech Republic

Employment & Professional experience

2001–2002 HSLMC, University of Cambridge, Cambridge, UK, Magnetic Resonance imaging of soil-water phenomena

2002 University of Hawaii, research assistant at Water Resources Research Center (3 months)

2003 Universitat Politecnica de Valencia, Dpto. de Ingeniería Hidráulica y Medio Ambiente (3 months)

2003–2004 University of Hawaii, post-doctoral researcher at Water Resources Research Center. Research on leaching of pesticides and pharmaceutical compounds in tropical soils (1 year)

2003–present Czech Technical Univ. in Prague, Faculty of Civil Engineering, researcher and assistant professor at Department of Irrigation, Drainage and Landscape Engineering

Recent research activities

Experimental research on preferential flow, unstable flow and contaminant transport in the vadose zone; noninvasive imaging techniques, numerical modeling of soil water flow and transport in the unsaturated zone.

2011 – 2014 *principal investigator,* project funded by Technology Agency of the Czech Republic, no. TA01021844, "Multi-point automated disk infiltrometer and methodology for routine measurements of infiltration capacity of soils"

2009, 2010 *principal investigator*, neutron imaging of soils supported by Paul Scherrer Institute, Switzerland, under proposals no. 20100526 and 20090465

2008 – 2012 *principal investigator*, project funded by Czech Science Foundation no. 103/08/1552 Water flow and solute transport in porous media with the presence of discontinuous gas phase

2005 – 2007 *key investigator* post-doctoral project funded by Ministry of Education and Youth of the Czech Republic, no. 1K05024 Influence of the entrapped air on preferential flow and contaminant transport in heterogeneous soils.

Recent participation (2006 – present) in 7 research projects funded by GACR, AVCR, MZP and MZE

Selected publications

Sněhota, M., Robovská, A., Císlerová, M., (2002): Automated set-up designed to measure hydraulic parameters in heterogeneous soil close to saturation. Journal of Hydrology and Hydromechanics, 50(3), 247-257.

Sněhota M., Císlerová M., (2005) Laboratory infiltration-outflow experiment monitored by magnetic resonance imaging (in Czech), Journal of Hydrology and Hydromechanics, 53(1), 54 – 62, 2005

Chen, J., Lichwa, J., Sněhota, M., Mohanty, S., Ray C., (2006) Determination of hormones and non-ionic surfactant degradation products in small-volume aqueous samples from soil columns using LC-ESI-MS-MS and GC-MS, Chromatographia 64(7-8): 413-418

Sněhota M, Sobotkova, M, Císlerová M., (2008), Impact of the entrapped air on water flow and solute transport in heterogeneous soil: Experimental set-up. Journal of Hydrology and Hydromechanics 56(4), 247-256

Sněhota M, Císlerová M., Amin, M.H.G., Hall L.D. (2010) Tracing the entrapped air in heterogeneous soil by means of magnetic resonance imaging, Vadose Zone Journal 9(2), 373-384

Jelínková V., Sněhota M., Pohlmeier A., van Dusschoten D., Císlerová M., (2011). Effects of entrapped residual air bubbles on tracer transport in heterogeneous soil: Magnetic resonance imaging study. Organic Geochemistry (in print)